

Supplemental material for: Fundamental limits on the rate of bacterial cell division

Nathan M. Belliveau^{1, †}, Griffin Chure^{2, †}, Christina L. Hueschen³, Hernan G. Garcia⁴, Jane Kondev⁵, Daniel S. Fisher⁶, Julie A. Theriot^{1, 7}, Rob Phillips^{8, 9, *}

***For correspondence:**

[†]These authors contributed equally to this work

¹Department of Biology, University of Washington, Seattle, WA, USA; ²Department of Applied Physics, California Institute of Technology, Pasadena, CA, USA; ³Department of Chemical Engineering, Stanford University, Stanford, CA, USA; ⁴Department of Molecular Cell Biology and Department of Physics, University of California Berkeley, Berkeley, CA, USA; ⁵Department of Physics, Brandeis University, Waltham, MA, USA; ⁶Department of Applied Physics, Stanford University, Stanford, CA, USA; ⁷Allen Institute for Cell Science, Seattle, WA, USA; ⁸Division of Biology and Biological Engineering, California Institute of Technology, Pasadena, CA, USA; ⁹Department of Physics, California Institute of Technology, Pasadena, CA, USA; * Address correspondence to phillips@pboc.caltech.edu

15 Contents

16	Summary of Proteome Data: Experimental Details	3
17	Fluorescence based measurements	3
18	Ribosomal profiling measurements	3
19	Mass spectrometry measurements	4
20	Summary of Proteomic Data	4
21	Estimation of Cell Size, Surface Area	5
22	Estimation of Total Protein Content per Cell	6
23	Additional Considerations of Schmidt <i>et al.</i> Data Set	7
24	Effect of cell volume on reported absolute protein abundances	9
25	Relaxing assumption of constant protein concentration across growth conditions	10
26	Experimental measurements of total protein from Basan <i>et al.</i> 2015.	11
27	Extending Estimates to a Continuum of Growth Rates	11
28	Estimation of the total cell mass	12
29	Complex Abundance Scaling With Cell Volume	12
30	A Relation for Complex Abundance Scaling With Surface Area	13
31	Number of Lipids	13
32	Number of Murein Monomers	13
33	Complex Abundance Scaling With Number of Origins	14

Table 1. Overview of proteomic data sets.

Author	Method	Reported Quantity
Taniguchi <i>et al.</i> (2010)	YFP-fusion, cell fluorescence	fg/copies per cell
Valgepea <i>et al.</i> (2012)	mass spectrometry	fg/copies per cell
Peebo <i>et al.</i> (2014)	mass spectrometry	fg/copies per fl
Li <i>et al.</i> (2014)	ribosomal profiling	fg/copies per cell ^a
Soufi <i>et al.</i> (2015)	mass spectrometry	fg/copies per cell
Schmidt <i>et al.</i> (2016)	mass spectrometry	fg/copies per cell ^b

a. The reported values assume that the proteins are long-lived compared to the generation time but are unable to account for post-translational modifications that may alter absolute protein abundances.

b. This mass spectrometry approach differs substantially from the others since in addition to the relative proteome-wide abundance measurements, the authors performed absolute quantification of 41 proteins across all growth conditions (see Section *Additional Considerations of Schmidt et al. Data Set* for more details on this).

Summary of Proteome Data: Experimental Details

Here we provide a brief summary of the experiments behind each proteomic data sets. The purpose of this section is to better identify the steps taken by the authors to arrive at absolute protein abundances. In the following section (Section *Summary of Proteomic Data*) we will then provide a summary of the final protein abundance measurements that were used for in the main text. Table 1 provides an overview of the main data sets that we considered. These are predominately mass spectrometry-based, with the exception of the work from Li *et al.* (2014) which used ribosomal profiling, and the fluorescence-based counting done in Taniguchi *et al.* (2010).

Fluorescence based measurements

In the work of Taniguchi *et al.* (2010), the authors used a chromosomal YFP fusion library where individual strains have a specific gene tagged with a YFP-coding sequence. 1018 of 1400 attempted strains were used in their work. For each strain, a fluorescence microscope was used to collect cellular YFP intensities. Through automated image analysis, the authors normalized intensity measurements by cell size to account for the change in size and expression variability across the cell cycle. YFP intensities were also corrected for cellular autofluorescence, and final absolute protein levels were determined by a calibration with single-molecule fluorescence intensities, performed separately using a purified YFP solution.

Ribosomal profiling measurements

The work of Li *et al.* (2014) takes a sequencing based approach to estimate protein abundance. Ribosomal profiling, which refers to the deep sequencing of ribosome-protected mRNA fragments, provides a quantitative measurement of the protein synthesis rate. As long as the protein life-time is long relative to the cell doubling time, it is possible to also estimate absolute protein copy numbers.

To perform ribosomal profiling, ribosome-protected mRNA is extracted from cell lysate and selected on a denaturing polyacrylamide gel, and sequences are obtained by deep sequencing (15–45 nt long fragments collected and sequenced by using an Illumina HiSeq 2000 in Li *et al.* (2014)). Counts of ribosome footprints from the sequencing data are corrected empirically for position-dependent biases in ribosomal density across each gene, as well as dependencies on specific sequences including the Shine-Dalgarno sequence. These data-corrected ribosome densities represent relative protein synthesis rates.

Absolute protein synthesis rates are obtained by multiplying the relative rates by the total cellular protein per cell. The total protein per unit volume was determined with the Lowry method

to quantify total protein, calibrated against bovine serum albumin (BSA). By counting colony-forming units following serial dilution of their cell cultures, they then calculated the total protein per cell. The absolute protein synthesis rate has units of proteins per generation, and for stable proteins will also correspond to the protein copy number per cell.

Mass spectrometry measurements

Perhaps not surprisingly, the data is predominantly mass spectrometry based. This is largely due to tremendous improvements in the sensitivity of mass spectrometers, as well as improvements in sample preparation and data analysis pipelines. It is now a relatively routine task to extract protein from a cell and quantify the majority of proteins by shotgun proteomics. In general, this involved lysing cells, enzymatically digesting the proteins into short peptide fragments, and then introducing them into the mass spectrometer (commonly employing liquid chromatography and electrospray ionization), which itself can have multiple rounds of detection and further fragmentation of the peptides.

Most quantitative experiments rely on labeling protein with stable isotopes, which allow multiple samples to be measured simultaneously by the mass spectrometer. By combining samples of known total protein abundance (i.e. one sample of interest, and one reference), it is possible to determine relative protein abundances. With relative protein abundances in hand, absolute protein abundances can be estimated following the same approach used above for ribosomal profiling, which is to multiply each relative abundance measurement by the total cellular protein per cell. This is the approach taken by *Valgepea et al. (2013)* and *Peebo et al. (2015)*, with relative protein abundances determined based on the relative peptide intensities (label free quantification 'LFQ' intensities). For the data of *Valgepea et al. (2013)*, total protein per cell was determined by measuring total protein by the Lowry method, and counting colony-forming units following serial dilution. For the data from *Peebo et al. (2015)*, the authors did not determine cell quantities and instead report the cellular protein abundances in protein per unit volume by assuming a mass density of 1.1 g/ml, with a 30% dry mass fraction.

A key distinction in the mass spectrometry work of *Schmidt et al. (2016)* is that in addition to determining relative abundance, they performed absolute quantification of 41 enzymes covering over four orders of magnitude in cellular abundance. Here, a synthetic peptide was generated for each of the 41 proteins, doped into each protein sample, and used to provide an calibration between measured mass spectrometry intensities and absolute protein abundances. These absolute measurements, determined for every growth condition considered in their work, were then used as a calibration curve to convert proteomic-wide relative abundances into absolute protein abundance per cell. A more extensive discussion of the *Schmidt et al. (2016)* data set can be found in Section Additional Considerations of Schmidt *et al.* Data Set.

Summary of Proteomic Data

In the work of the main text we only used the data from *Valgepea et al. (2013)*; *Li et al. (2014)*; *Peebo et al. (2015)*; *Schmidt et al. (2016)*. As shown in *Figure 1(A)*, the reported total protein abundances in the work of *Taniguchi et al. (2010)* and *Soufi et al. (2015)* differed quite substantially from the other work. For the work of *Taniguchi et al. (2010)* this is in part due to a lower coverage in total proteomic mass quantified, though we also noticed that most proteins appear to be undercounted when compared to the other data.

Figure 1(B) summarizes the total protein mass for each data point in our final compiled data set. Here we note that protein abundances were all scaled so they followed an identical growth rate-dependent change in total protein mass. While our inclination initially was to leave reported copy numbers untouched, a notable discrepancy between the total protein per cell between *Schmidt et al. (2016)* and the other data sets (see fast growth conditions in *Figure 1(A)*) forced us to dig deeper into those measurements. The particular scaling in the total protein content observed in the data from *Schmidt et al. (2016)* appears to be due to their assumptions on cell size and we provide

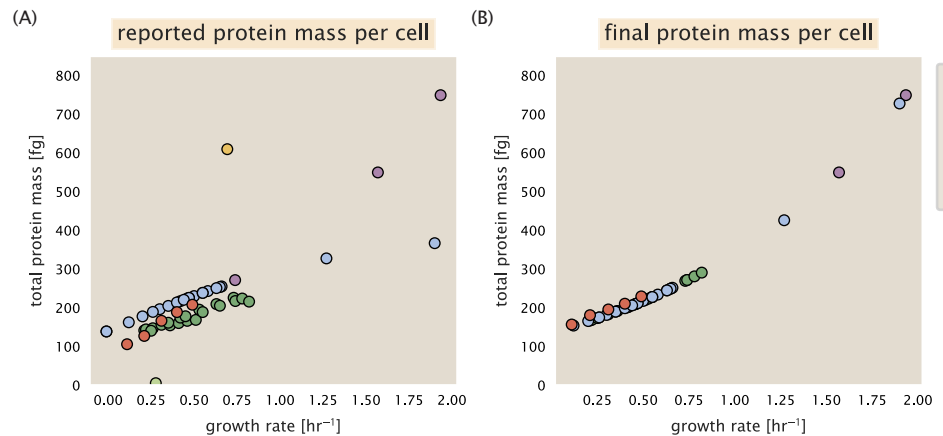


Figure 1. Summary of the growth-rate dependent total protein abundance for each data set. (A) Total protein abundance per cell as original reported in the data sets of *Taniguchi et al. (2010)*; *Valgepea et al. (2013)*; *Li et al. (2014)*; *Soufi et al. (2015)*; *Peebo et al. (2015)*; *Schmidt et al. (2016)*. Note that the data from *Peebo et al. (2015)* only reported protein abundances per unit volume and total protein per cell was found by multiplying these by the growth-rate dependent cell size as determined by *Si et al. (2017)*. (B) Adjusted total protein abundances across the proteomic data sets are summarized. Protein abundances were adjusted so that all data shared a common set of growth-rate dependent total protein per cell and cellular protein concentration following the cell size expectations of *Si et al. (2017)* (see section on Estimation of Cell Size, Surface Area for further details).

a more extensive discussion and analysis of that data set in section Additional Considerations of Schmidt *et al.* Data Set. As a compromise, and in an effort to treat all data equally, we instead scaled all protein abundance values from each data set using a common model growth-rate dependent cell size and protein concentration based on the size data available from *Si et al. (2017)*. We consider those details in section Estimation of Cell Size, Surface Area that follows.

In *Figure 2* we also show the total proteomic coverage and overlap of proteins quantified across each data set. Here we have used an UpSet diagram (*Lex et al., 2014*) to compare the data. Overall, the overlap in quantified proteins is quite good, with 1157 proteins with abundances values quantified in all data sets. The sequencing based approach of *Li et al. (2014)* has substantially higher coverage compared to the mass spectrometry data sets (3394 genes versus the 2041 genes quantified in the work of *Schmidt et al. (2016)*). However, in terms of total protein mass, the data from *Li et al. (2014)*; *Schmidt et al. (2016)*; *Peebo et al. (2015)* each quantify roughly equivalent total protein. We find that the total protein quantified in *Valgepea et al. (2013)* is 90-95 % of the total protein mass (when using the data from *Schmidt et al. (2016)* as a reference).

Estimation of Cell Size, Surface Area

Since most of the proteomic data sets lack cell size measurements, we chose instead to use a common set of size measurements for any analysis requiring cell size or surface area. Since each of the data sets used either K-12 MG1655 or its derivative, BW25113 (from the lab of Barry L. Wanner; the parent strain of the Keio collection (*Datsenko and Wanner, 2000*; *Baba et al., 2006*)), we fit the MG1655 cell size data from *Si et al. 2017, 2019* using the `optimize.curve_fit` function from the Scipy python package (*Virtanen et al., 2020*).

The size data is shown in *Figure 3*(A) and (B), for the cell length and width, respectively. The length data was well described by the exponential function $0.5 e^{1.09 \cdot \lambda} + 1.76 \mu\text{m}$, while the width data was well described by $0.64 e^{0.24 \cdot \lambda} \mu\text{m}$. In order to estimate cell size we take the cell as a cylinders with two hemispherical ends (*Si et al., 2017*; *Basan et al., 2015*). Specifically, cell size (or volume) is

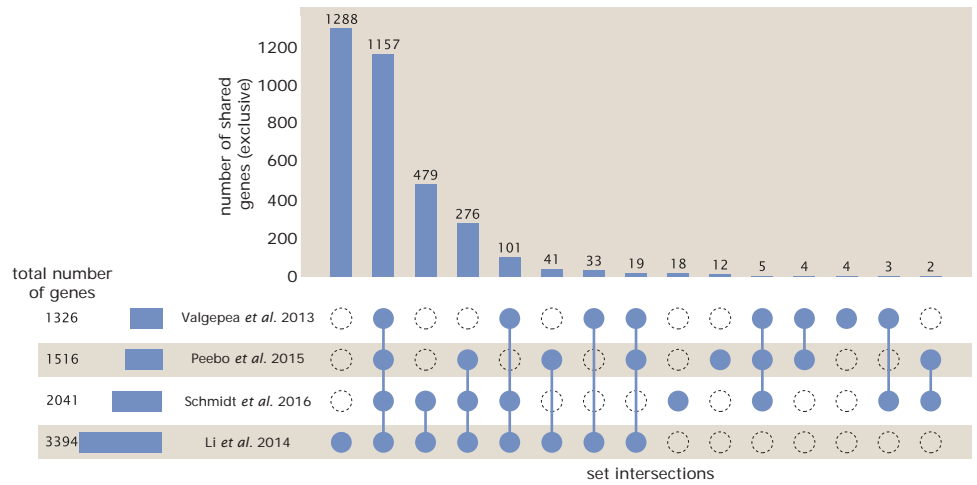


Figure 2. Comparison of proteomic coverage across different data sets. An UpSet diagram (Lex et al., 2014) summarizes the total number of protein coding genes whose protein abundance was reported in the data sets of Valgepea et al. (2013); Li et al. (2014); Schmidt et al. (2016); Peebo et al. (2015). The total number of genes reported in each individual data set are noted on the bottom left, while their overlap is summarized in the bar chart. Each column here refers to the intersection of a set of data sets identified by blue circles.

139 estimated from,

$$V = \pi \cdot r^2 \cdot (l - 2r/3), \quad (1)$$

140 where r is half the cell width. A best fit to the data is described by $0.533 e^{1.037 \cdot \lambda} \mu\text{m}^3$. Calculation of
141 the cell surface area is given by,

$$S = \eta \cdot \pi \left(\frac{\eta \cdot \pi}{4} - \frac{\pi}{12} \right)^{-2/3} V^{2/3}, \quad (2)$$

142 where η is the aspect ratio ($\eta = l/w$) (Ojkic et al., 2019).

143 Estimation of Total Protein Content per Cell

144 In order to estimate total protein per cell for a particular growth rate, we begin by estimating the cell
145 size from the fit shown in Figure 3(C) ($0.533 e^{1.037 \cdot \lambda} \mu\text{m}^3$). We then estimate the total protein
146 content from the total dry mass of the cell. Here we begin by noting that for almost the entire range
147 of growth rates considered here, protein, DNA, and RNA were reported to account for at least 90 %
148 of the dry mass (Basan et al. (2015)). The authors also found that the total dry mass concentration
149 was roughly constant across growth conditions. Under such a scenario, we can calculate the total
150 dry mass concentration for protein, DNA, and RNA, which is given by $1.1 \text{ g/ml} \times 30 \% \times 90 \%$ or about
151 $[M_p] = 300 \text{ fg per fl}$. Multiplying this by our prediction of cell size gives the total dry mass per cell.

152 However, even if dry mass concentration is relatively constant across growth conditions, it
153 is not obvious how protein concentration might vary due to the substantial increase in rRNA at
154 faster growth rates (Dai et al. (2016)). This is a well-documented result that arises from an increase
155 in ribosomal abundance at faster growth rates (Scott et al. (2010)). To proceed therefore rely on
156 experimental measurements of total DNA content per cell that also come from Basan et al., and RNA
157 to protein ratios that were measured in Dai et al. (and cover the entire range of growth conditions
158 considered here). These are reproduced in Figure 4(A) and (B), respectively.

159 Assuming that the protein, DNA, and RNA account for 90 % of the total dry mass, the protein
160 mass can then determined by first subtracting the experimentally measured DNA mass, and then
161 using the experimental estimate of the RNA to protein ratio. The total protein per cell is will be

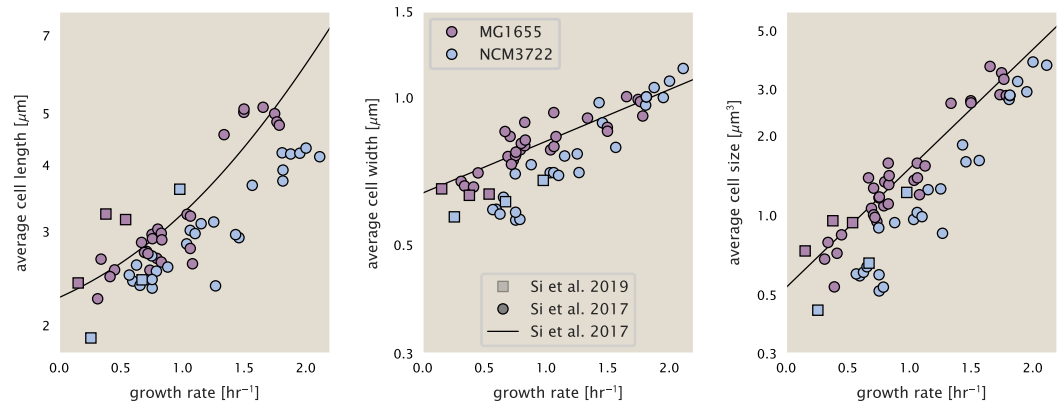


Figure 3. Summary of size measurements from Si *et al.* 2017, 2019. Cell lengths and widths were measured from cell contours obtained from phase contrast images, and refer to the long and short axis respectively. (A) Cell lengths and (B) cell widths show the mean measurements reported (they report 140-300 images and 5,000-30,000 for each set of samples; which likely means about 1,000-5,000 measurements per mean value reported here since they considered about 6 conditions at a time). Fits were made to the MG1655 strain data; length: $0.5 e^{1.09 \cdot \lambda} + 1.76 \mu\text{m}$, width: $0.64 e^{0.24 \cdot \lambda} \mu\text{m}$. (C) Cell size, V , was calculated as cylinders with two hemispherical ends (Equation 1). The MG1655 strain data gave a best fit of $0.533 e^{1.037 \cdot \lambda} \mu\text{m}^3$.

related to the summed RNA and protein mass by,

$$M_p = \frac{[M_p + M_{RNA}]}{1 + (RP_{ratio})}. \quad (3)$$

(RP_{ratio} refers to the RNA to protein ratio as measured by Dai *et al.*. In Figure 4(C) we plot the estimated cellular concentrations for protein, DNA, and RNA from these calculations, and in Figure 4(D) we plot their total expected mass per cell. This later quantity is the growth rate-dependent total protein mass that was used to estimate total protein abundance across all data sets (and summarized in Figure 1(B)).

Additional Considerations of Schmidt *et al.* Data Set

While the data set from Schmidt *et al.* (2016) remains a heroic effort that our lab continues to return to as a resource, there were steps taken in their calculation of protein copy number that we felt needed further consideration. In particular, the authors made an assumption of constant cellular protein concentration across all growth conditions and used measurements of cell volume that appear inconsistent with an expected exponential scaling of cell size with growth rate that is well-documented in *E. coli* (Schaechter *et al.* (1958); Taheri-Araghi *et al.* (2015); Si *et al.* (2017)).

We begin by looking at their cell volume measurements, which are shown in blue in Figure 5. As a comparison, we also plot cell sizes reported in three other recent papers: measurements from Taheri-Araghi *et al.* and Si *et al.* come from the lab of Suckjoon Jun, while those from Basan *et al.* come from the lab of Terence Hwa. Each set of measurements used microscopy and cell segmentation to determine the length and width, and then calculated cell size by treating the cell as a cylinder with two hemispherical ends. While there is notable discrepancy between the two research groups, Basan *et al.* found that this came specifically from uncertainty in determining the cell width, which is prone to inaccuracy given the small cell size and optical resolution limits (further described in their supplemental text). Perhaps the more concerning point is that while each of these alternative measurements show an exponential increase in cell size at faster growth rates, the measurements used by Schmidt *et al.* appear to plateau. This resulted in an analogous trend in their final reported total cellular protein per cell as shown in Figure 6 (purple data points), and is in disagreement with other measurements of total protein at these growth rates (Basan *et al.*, 2015).

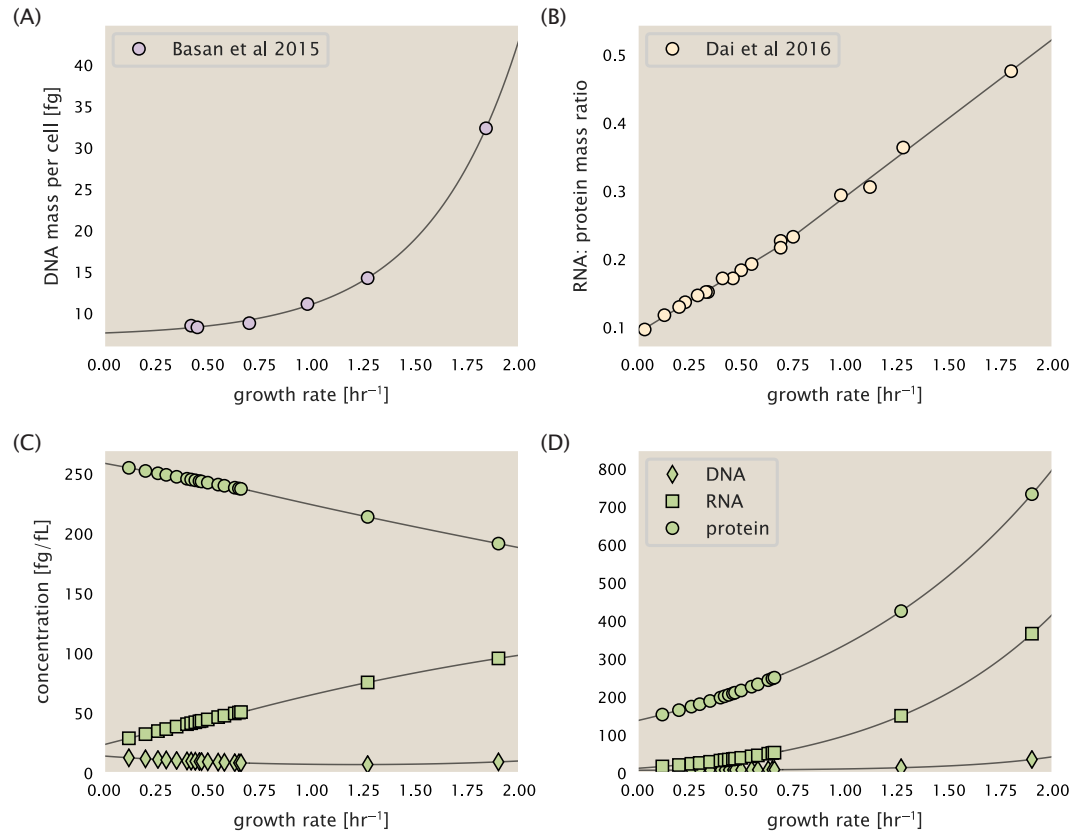


Figure 4. Empirical estimate of cellular protein, DNA, and RNA as a function of growth rate. (A) Measured DNA mass per cell as a function of growth rate, reproduced from Basan *et al.* 2015. The data was fit to an exponential curve (DNA mass in fg per cell is given by $0.42 e^{2.23 \cdot \lambda} + 7.2$ fg per cell, where λ is the growth rate in hr⁻¹). (B) RNA to protein measurements as a function of growth rate. The data was fit to two lines: for growth rates below 0.7 hr⁻¹, the RNA/protein ratio is $0.18 \cdot \lambda + 0.093$, while for growth rates faster than 0.7 hr⁻¹ the RNA/protein ratio is given by $0.25 \cdot \lambda + 0.035$. For (A) and (B) cells are grown under varying levels of nutrient limitation, with cells grown in minimal media with different carbon sources for the slowest growth conditions, and rich-defined media for fast growth rates. (C) Predictions of cellular protein, DNA, and RNA concentration. (D) Total cellular mass predicted for protein, DNA, and RNA using the cell size predictions from Si *et al.*. Symbols (diamond: DNA, square: RNA, circle: protein) show estimated values of mass concentration and mass per cell for the specific growth rates in Schmidt *et al.* (2016).

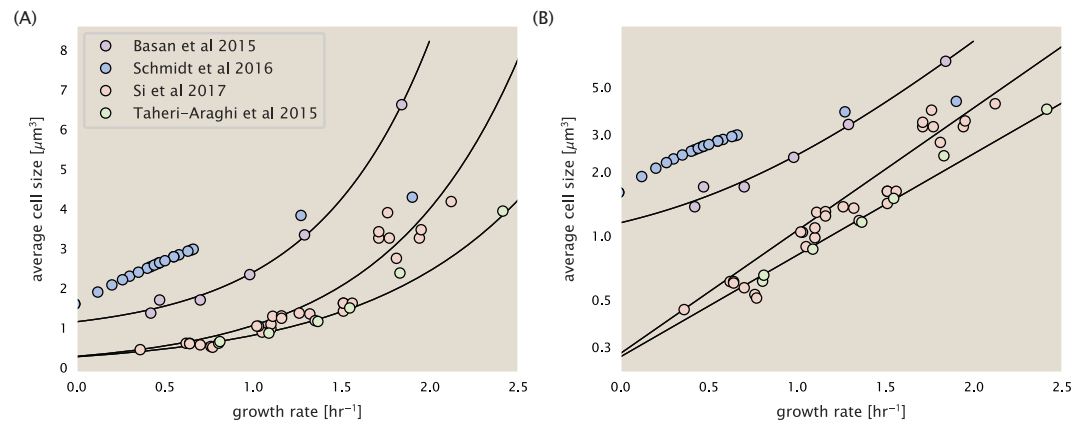


Figure 5. Measurements of cell size as a function of growth rate. (A) Plot of the reported cell sizes from several recent papers. The data in blue come from Volkmer and Heinemann, 2011 (*Volkmer and Heinemann (2011)*) and were used in the work of Schmidt *et al.*. Data from the lab of Terence Hwa are shown in purple (*Basan et al. (2015)*), while the two data sets shown in green and red come from the lab of Suckjoon Jun (*Taheri-Araghi et al. (2015)*; *Si et al. (2017)*). (B) Same as in (A) but with the data plotted on a logarithmic y-axis to highlight the exponential scaling that is expected for *E. coli*.

Since it is not obvious how measurements of cell size might have influenced their reported protein abundances, in the following subsections we begin by considering this calculation. We then consider three different approaches to estimate the growth-rate dependent total protein mass to compare with those values reported by *Schmidt et al. (2016)*. The results of this are summarized in *Figure 5(B)*, with the original values from both *Schmidt et al. (2016)* and *Li et al. (2014)* shown in *Figure 5(A)* for reference. For most growth conditions, we find that total protein expectations are not expected to change dramatically. However, for the fastest growth conditions, with glycerol + supplemented amino acids, and LB media, all estimates are substantially higher than those originally reported and justify why we readjusted the protein abundance to be more consistent with this alternative expectation (which is described in section Estimation of Cell Size, Surface Area).

Effect of cell volume on reported absolute protein abundances

The authors calculated proteome-wide protein abundance by first determining absolute abundances of 41 pre-selected proteins, which relied on adding synthetic heavy reference peptides into their protein samples at known abundance (with proteins selected to cover the range of expected copy numbers). This absolute quantitation was performed in replicate for each growth condition. Separately, the authors also performed a more conventional mass spectrometry measurement for samples from each growth condition, which attempted to maximize the number of quantified proteins but only provided relative abundances based on peptide intensities. Finally, using their 41 proteins with absolute abundances already determined, they then created calibration curves with which to relate their relative intensity to absolute protein abundance for each growth condition. This allowed them to estimate absolute protein abundance for all proteins detected in their proteome-wide data set. Combined with their flow cytometry cell counts, they were then able to determine absolute abundance of each protein detected on a per cell basis.

While this approach provided absolute abundances, another necessary step needed to arrive at total cellular protein is to account for any protein loss during their various protein extraction steps. Here the authors attempted to determine total protein separately using a BCA protein assay. In personal communications, it was noted that determining reasonable total protein abundances by BCA across their array of growth conditions was particularly troublesome. Instead, they noted confidence in their total protein measurements for cells grown in M9 minimal media + glucose and used this as a reference point with which to estimate the total protein for all other growth

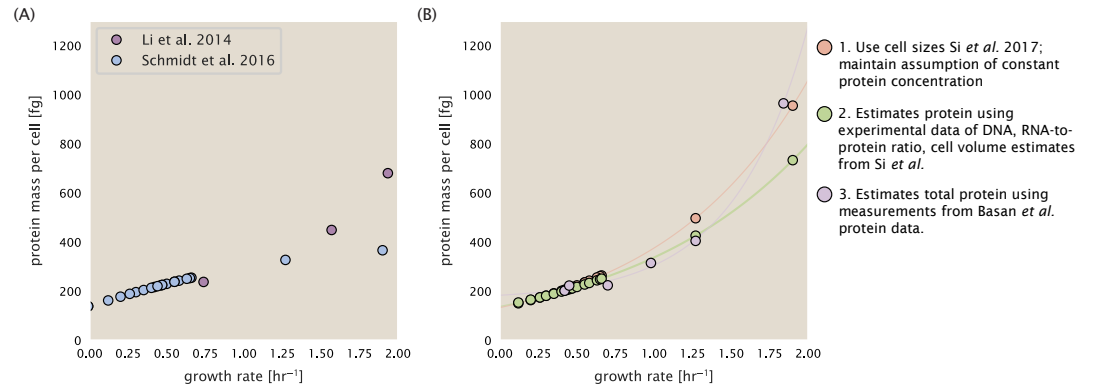


Figure 6. Alternative estimates of total cellular protein for the growth conditions considered in Schmidt et al. (A) The original protein mass from Schmidt et al. and Li et al. are shown in purple and blue, respectively. (B) Three alternative estimates of total protein per cell. 1. *light red*: Rescaling of total protein mass assuming a growth rate independent protein concentration and cell volumes estimated from Si et al. 2017. 2. *light green*: Rescaling of total protein mass using estimates of growth rate-dependent protein concentrations and cell volumes estimated from Si et al. 2017. Total protein per cell is calculated by assuming a 1.1 g/ml cellular mass density, 30% dry mass, with 90% of the dry mass corresponding to DNA, RNA, and protein (Basan et al., 2015). See Estimation of Total Protein Content per Cell for details on calculation. 3. *light purple*: Rescaling of total protein mass using the experimental measurements from Basan et al. 2015.

conditions.

For cells grown in M9 minimal media + glucose an average total mass of $M_p = 240$ fg per cell was measured. Using their reported cell volume, reported as $V_{orig} = 2.84$ fl, a cellular protein concentration of $[M_p]_{orig} = M_p/V_{orig} = 85$ fg/fl. Now, taking the assumption that cellular protein concentration is relatively independent of growth rate, they could then estimate the total protein mass for all other growth conditions from,

$$M_{p,i} = [M_p]_{orig} \cdot V_i \quad (4)$$

where $M_{p,i}$ represents the total protein mass per cell and V_i is the cell volume for each growth condition i as measured in Volkmer and Heinemann, 2011. Here the thinking is that the values of $M_{p,i}$ reflects the total cellular protein for growth condition i , where any discrepancy from their absolute protein abundance is assumed to be due to protein loss during sample preparation. The protein abundances from their absolute abundance measurements noted above were therefore scaled to their estimates and are shown in Figure **Figure 6** (purple data points).

If we instead consider the cell volumes predicted in the work of Si et al., we again need to take growth in M9 minimal media + glucose as a reference with known total mass, but we can follow a similar approach to estimate total protein mass for all other growth conditions. Letting $V_{Si_glu} = 0.6$ fl be the predicted cell volume, the cellular protein concentration becomes $[M_p]_{Si} = M_p/V_{Si_glu} = 400$ fg/fl. The new total protein mass per cell can then be calculated from,

$$M'_{p,i} = [M_p]_{Si} \cdot V_{Si,i} \quad (5)$$

where $M'_{p,i}$ is the new protein mass prediction, and $V_{Si,i}$ refers to the new volume prediction for each condition i . These are shown as red data points in Figure **Figure 6**(B).

Relaxing assumption of constant protein concentration across growth conditions

We next relax the assumption that cellular protein concentration is constant and instead, attempt to estimate it using experimental data. Here we use the estimation of total protein mass per cell detailed in section Estimation of Total Protein Content per Cell for all data points in the **Schmidt**

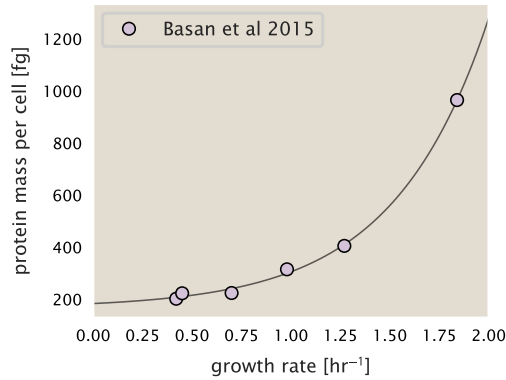


Figure 7. Total cellular protein reported in Basan *et al.* 2015. Measured protein mass as a function of growth rate as reproduced from Basan *et al.* 2015, with cells grown under different levels of nutrient limitation. The data was fit to an exponential curve where protein mass in fg per cell is given by $14.65 e^{2.180 \cdot \lambda} + 172$ fg per cell, where λ is the growth rate in hr^{-1}).

242 *et al.* (2016) data set. The green data points in *Figure 6(B)* show this prediction, and this represents
 243 the approach used to estimate total protein per cell for all data sets.

244 **Experimental measurements of total protein from Basan *et al.* 2015.**

245 One of the challenges in our estimates in the preceding sections is the need to estimate protein
 246 concentration and cell volumes. These are inherently difficult to accurately due to the small size
 247 of *E. coli*. Indeed, for all the additional measurements of cell volume included in *Figure 5*, no
 248 measurements were performed for cells growing at rates below 0.5 hr^{-1} . It therefore remains to be
 249 determined whether our extrapolated cell volume estimates are appropriate, with the possibility
 250 that the logarithmic scaling of cell size might break down for slower growth.

251 In our last approach we therefore attempt to estimate total protein using experimental data
 252 that required no estimates of concentration or cell volume. Specifically, in the work of Basan *et al.*,
 253 the authors measured total protein per cell for a broad range of growth rates (reproduced in *Figure*
 254 *Figure 7*). These were determined by first measuring bulk protein from cell lysate, measured by the
 255 colorimetric Biuret method (You *et al.* (2013)), and then abundance per cell was calculated from
 256 cell counts from either plating cells or a Coulter counter. While it is unclear why Schmidt *et al.* was
 257 unable to take a similar approach, the results from Basan *et al.* appear more consistent with our
 258 expectation that cell mass will increase exponentially with faster growth rates. In addition, although
 259 they do not consider growth rates below about 0.5 hr^{-1} , it is interesting to note that the protein
 260 mass per cell appears to plateau to a minimum value at slow growth. In contrast, our estimates
 261 using cell volume so far have predicted that total protein mass should continue to decrease slightly
 262 for slower growing cells. By fitting this data to an exponential function dependent on growth rate,
 263 we could then estimate the total protein per cell for each growth condition considered by Schmidt
 264 *et al.* (2016). These are plotted as red data points in *Figure 6(B)*.

265 **Extending Estimates to a Continuum of Growth Rates**

266 In the main text, we considered a standard stopwatch of 5000 s to estimate the abundance of
 267 the various protein complexes considered. In addition to point estimates, we also showed the
 268 estimate as a function of growth rate as transparent grey curves. In this section, we elaborate
 269 on this continuum estimate, giving examples of estimates that scale with either cell volume, cell
 270 surface area, or number of origins of replication.

Estimation of the total cell mass

For many of the processes estimated in the main text we relied on a cellular dry mass of ≈ 300 fg from which we computed elemental and protein fractions using knowledge of fractional composition of the dry mass. At modest growth rates, such as the 5000 s doubling time used in the main text, this is a reasonable number to use as the typical cell mass is ≈ 1 pg and *E. coli* cells can be approximated as 70% water by volume. However, as we have shown in the preceding sections, the cell size and therefore cell volume is highly dependent on the growth rate. This means that a dry mass of 300 fg cannot be used reliably across all growth rates.

Rather, using the phenomenological description of cell volume scaling exponentially with growth rate, and using a rule-of-thumb of a cell buoyant density of ≈ 1.1 pg / fL (BNID: 103875), we can calculate the cell dry mass across a range of physiological growth rates as

$$m_{\text{cell}} \approx \rho V(\lambda) \approx \rho a e^{\lambda * b} \quad (6)$$

where a and b are constants with units of μm^3 and hr, respectively. The value of these constants can be estimated from the careful volume measurements performed by *Si et al. (2017)*, as is described in the previous section.

Complex Abundance Scaling With Cell Volume

Several of the estimates performed in the main text are implicitly dependent on the cell volume. This includes processes such as ATP synthesis and, most prominently, the transport of nutrients. Of the latter, we estimated the number of transporters that would be needed to shuttle enough carbon, phosphorus, and sulfur across the membrane to build new cell mass. To do so, we used elemental composition measurements combined with a 300 fg cell dry mass to make the point estimate. As we now have a means to estimate the total cell mass as a function of volume, we can generalize these estimates across growth rates.

Rather than discussing the particular details of each transport system, we will derive this scaling expression in very general terms. Consider we wish to estimate the number of transporters for some substance X , which has been measured to be make up some fraction of the dry mass θ_X . If we assume that, irrespective of growth rate, the cell dry mass is $\approx 30\%$ of the total cell mass, we can state that the total mass of substance X as a function of growth rate is

$$m_X \approx 0.3 \times \rho V(\lambda) \theta_X, \quad (7)$$

where we have used $\rho V(\lambda)$ as an estimate of the total cell mass, defined in **Equation 6**. To convert this to the number of units N_X of substance X in the cell, we can use the formula weight w_X of a single unit of X in conjunction with **Equation 7**,

$$N_X \approx \frac{m_X}{w_X}. \quad (8)$$

To estimate the number of transporters needed, we make the approximation that loss of units of X via diffusion through porins or due to the permeability of the membrane is negligible and that a single transporter complex can transport substance X at a rate r_X . As this rate r_X is in units of X per time per transporter, we must provide a time window over which the transport process can occur. This is related to the cell doubling time τ , which can be calculated from the growth rate λ as $\tau = \log(2)/\lambda$. Putting everything together, we arrive at a generalized transport scaling relation of

$$N_{\text{transporters}}(\lambda) = \frac{0.3 \times \rho V(\lambda) \theta_X}{w_X r_X \tau}. \quad (9)$$

This function is used to draw the continuum estimates for the number of transporters seen in Figures 2 and 3 as transparent grey curves. Occasionally, this continuum scaling relationship will not precisely agree with the point estimate outlined in the main text. This is due to the fact that we make an initial approximation made of a dry cell mass of ≈ 300 fg for the point estimate while we

consider more precise values in the continuum estimate. We note, however, that both this scaling relation and the point estimates are meant to describe the order-of-magnitude observed, and not the predict the exact values of the abundances.

Equation 9 is a very general relation for processes where the cell volume is the "natural variable" of the problem. This means that, as the cell increases in volume, the requirements for substance X also scale with volume rather than scaling with surface area, for example. So long as the rate of the process, the fraction of the dry mass attributable to the substance, and the formula mass of the substance is known, **Equation 9** can be used to compute the number of complexes needed. For example, to compute the number of ATP synthases per cell, **Equation 9** can be slightly modified to the form

$$N_{\text{ATP synthases}}(\lambda) = \frac{0.3 \times \rho V(\lambda) \theta_{\text{protein}} N_{\text{ATP}}}{w_{\text{AA}} r_{\text{ATP}} \tau}, \quad (10)$$

where we have included the term N_{ATP} to account for the number of ATP equivalents needed per amino acid for translation (≈ 4 , BNID: 114971), and w_{AA} is the average mass of an amino acid. The grey curves in Figure 4 of the main text were made using this type of expression.

A Relation for Complex Abundance Scaling With Surface Area

In our estimation for the number of complexes needed for lipid synthesis and peptidoglycan maturation, we used a particular estimate for the cell surface area ($\approx 5 \mu\text{m}^2$, BNID: 101792) and the fraction of dry mass attributable to peptidoglycan ($\approx 3\%$, BNID: 101936). Both of these values come from glucose-fed *E. coli* in balance growth. As we are interested in describing the scaling as a function of the growth rate, we must consider how these values scale with cell surface area, which is the natural variable for these types of processes. In the coming paragraphs, we highlight how we incorporate a condition dependent surface area in to our calculation of the number of lipids and murein monomers that need to be synthesized and crosslinked, respectively.

Number of Lipids

To compute the number of lipids as a function of growth rate, we make the assumption that some features, such as the surface area of a single lipid ($A_{\text{lipid}} \approx 0.5 \text{ nm}^2$, BNID: 106993) and the total fraction of the membrane composed of lipids ($\approx 40\%$, BNID: 100078) are independent of the growth rate. Using these approximations combined with **Equation 2**, and recognizing that each membrane is composed of two leaflets, we can compute the number of lipids as a function of growth rate as

$$N_{\text{lipids}}(\lambda) \approx \frac{4 \text{ leaflets} \times 0.4 \times \eta \pi \left(\frac{\eta \pi}{4} - \frac{\pi}{12} \right)^{-2/3} V(\lambda)^{2/3}}{A_{\text{lipid}}} \quad (11)$$

where η is the length-to-width aspect ratio and V is the cell volume.

Number of Murein Monomers

In calculation of the number of transpeptidases needed for maturation of the peptidoglycan, we used an empirical measurement that $\approx 3\%$ of the dry mass is attributable to peptidoglycan and that a single murein monomer is $m_{\text{murein}} \approx 1000 \text{ Da}$. While the latter is independent of growth rate, the former is not. As the peptidoglycan exists as a thin shell with a width of $w \approx 10 \text{ nm}$ encapsulating the cell, one would expect the number of murein monomers scales with the surface area of this shell. In a similar spirit to our calculation of the number of lipids, the total number of murein monomers as a function of growth rate can be calculated as

$$N_{\text{murein monomers}}(\lambda) \approx \frac{\rho_{\text{pg}} w \eta \pi \left(\frac{\eta \pi}{4} - \frac{\pi}{12} \right)^{-2/3} V(\lambda)^{2/3}}{m_{\text{murein}}}, \quad (12)$$

where ρ_{pg} is the density of peptidoglycan.

Complex Abundance Scaling With Number of Origins

While the majority of our estimates hinge on the total cell volume or surface area, processes related to the central dogma, namely DNA replication and synthesis of rRNA, depend on the number of chromosomes present in the cell. As discussed in the main text, the ability of *E. coli* to parallelize the replication of its chromosome by having multiple active origins of replication at a given is critical to synthesize enough rRNA, especially at fast growth rates. Derived in *Si et al. (2017)* and reproduced in the main text, the average number of origins of replication at a given growth rate can be calculated as

$$\langle \#ori \rangle \approx 2^{t_{cyc} \lambda / \ln 2} \quad (13)$$

where t_{cyc} is the total time of replication and division. We can make the approximation that $t_{cyc} \approx 70$ min, which is the time it takes two replisomes to copy an entire chromosome.

In the case of rRNA synthesis, the majority of the rRNA operons are surrounding the origin of replication. Thus, at a given growth rate λ , the average dosage of rRNA operons per cell D_{rRNA} is

$$D_{rRNA}(\lambda) \approx N_{rRNA \text{ operons}} \times 2^{t_{cyc} \lambda / \ln 2}. \quad (14)$$

This makes the approximation that *all* rRNA operons are localized around the origin. In reality, the operons are some distance away from the origin, making **Equation 14** an approximation.

In the main text, we stated that at the growth rate in question, there is ≈ 1 chromosome per cell. While a fair approximation, **Equation 13** illustrates that is not precisely true, even at slow growth rates. In estimating the number of RNA polymerases as a function of growth rate, we consider that regardless of the number of rRNA operons, they are all sufficiently loaded with RNA polymerase such that each operon produces one rRNA per second. Thus, the total number of RNA polymerase as a function of the growth rate can be calculated as

$$N_{RNA \text{ polymerase}}(\lambda) \approx L_{operon} D_{rRNA} \rho_{RNA \text{ polymerase}}, \quad (15)$$

where L_{operon} is the total length of an rRNA operon (≈ 4500 bp) and $\rho_{RNA \text{ polymerase}}$ is packing density of RNA polymerase on a given operon, taken to be 1 RNA polymerase per 80 nucleotides.

References

- Baba, T., Ara, T., Hasegawa, M., Takai, Y., Okumura, Y., Baba, M., Datsenko, K. A., Tomita, M., Wanner, B. L., and Mori, H. (2006). Construction of Escherichia coli K-12 in-frame, single-gene knockout mutants: the Keio collection. *Molecular Systems Biology*, 2(1):2460.
- Basan, M., Zhu, M., Dai, X., Warren, M., Sévin, D., Wang, Y.-P., and Hwa, T. (2015). Inflating bacterial cells by increased protein synthesis. *Molecular Systems Biology*, 11(10):836.
- Dai, X., Zhu, M., Warren, M., Balakrishnan, R., Patsalo, V., Okano, H., Williamson, J. R., Fredrick, K., Wang, Y.-P., and Hwa, T. (2016). Reduction of translating ribosomes enables Escherichia coli to maintain elongation rates during slow growth. *Nature Microbiology*, 2(2):16231.
- Datsenko, K. A. and Wanner, B. L. (2000). One-step inactivation of chromosomal genes in Escherichia coli K-12 using PCR products. *Proceedings of the National Academy of Sciences*, 97(12):6640–6645.
- Lex, A., Gehlenborg, N., Strobel, H., Vuilleumot, R., and Pfister, H. (2014). UpSet: visualization of intersecting sets. *IEEE Transactions on Visualization and Computer Graphics*, 20(12):1983–1992.
- Li, G.-W., Burkhardt, D., Gross, C., and Weissman, J. S. (2014). Quantifying absolute protein synthesis rates reveals principles underlying allocation of cellular resources. *Cell*, 157(3):624–635.
- Ojkic, N., Serbanescu, D., and Banerjee, S. (2019). Surface-to-volume scaling and aspect ratio preservation in rod-shaped bacteria. *eLife*, 8:642.
- Peebo, K., Valgepea, K., Maser, A., Nahku, R., Adamberg, K., and Vilu, R. (2015). Proteome reallocation in *Escherichia coli* with increasing specific growth rate. *Molecular BioSystems*, 11(4):1184–1193.
- Schaechter, M., Maaløe, O., and Kjeldgaard, N. O. (1958). Dependency on medium and temperature of cell size and chemical composition during balanced growth of *Salmonella typhimurium*. *Microbiology*, 19(3):592–606.

- 392 Schmidt, A., Kochanowski, K., Vedelaar, S., Ahrné, E., Volkmer, B., Callipo, L., Knoops, K., Bauer, M., Aebersold,
393 R., and Heinemann, M. (2016). The quantitative and condition-dependent *Escherichia coli* proteome. *Nature*
394 *Biotechnology*, 34(1):104–110.
- 395 Scott, M., Gunderson, C. W., Mateescu, E. M., Zhang, Z., and Hwa, T. (2010). Interdependence of cell growth and
396 gene expression: origins and consequences. *Science*, 330(6007):1099–1102.
- 397 Si, F., Li, D., Cox, S. E., Sauls, J. T., Azizi, O., Sou, C., Schwartz, A. B., Erickstad, M. J., Jun, Y., Li, X., and Jun, S. (2017).
398 Invariance of Initiation Mass and Predictability of Cell Size in *Escherichia coli*. *Current Biology*, 27(9):1278–1287.
- 399 Soufi, B., Krug, K., Harst, A., and Macek, B. (2015). Characterization of the *E. coli* proteome and its modifications
400 during growth and ethanol stress. *Frontiers in Microbiology*, 6:198.
- 401 Taheri-Araghi, S., Bradde, S., Sauls, J. T., Hill, N. S., Levin, P. A., Paulsson, J., Vergassola, M., and Jun, S. (2015).
402 Cell-size control and homeostasis in bacteria. *Current Biology*, 25(3):385–391.
- 403 Taniguchi, Y., Choi, P. J., Li, G.-W., Chen, H., Babu, M., Hearn, J., Emili, A., and Xie, X. S. (2010). Quantifying
404 *E. coli* proteome and transcriptome with single-molecule sensitivity in single cells. *Science (New York, N.Y.)*,
405 329(5991):533–538.
- 406 Valgepea, K., Adamberg, K., Seiman, A., and Vilu, R. (2013). *Escherichia coli* achieves faster growth by increasing
407 catalytic and translation rates of proteins. *Molecular BioSystems*, 9(9):2344.
- 408 Virtanen, P., Gommers, R., Oliphant, T. E., Haberland, M., Reddy, T., Cournapeau, D., Burovski, E., Peterson, P.,
409 Weckesser, W., Bright, J., van der Walt, S. J., Brett, M., Wilson, J., Jarrod Millman, K., Mayorov, N., Nelson, A. R. J.,
410 Jones, E., Kern, R., Larson, E., Carey, C., Polat, İ., Feng, Y., Moore, E. W., Vand erPlas, J., Laxalde, D., Perktold,
411 J., Cimrman, R., Henriksen, I., Quintero, E. A., Harris, C. R., Archibald, A. M., Ribeiro, A. H., Pedregosa, F., van
412 Mulbregt, P., and Contributors, S. . . (2020). SciPy 1.0: Fundamental Algorithms for Scientific Computing in
413 Python. *Nature Methods*, 17:261–272.
- 414 Volkmer, B. and Heinemann, M. (2011). Condition-Dependent Cell Volume and Concentration of *Escherichia coli*
415 to Facilitate Data Conversion for Systems Biology Modeling. *PLOS ONE*, 6(7):e23126.
- 416 You, C., Okano, H., Hui, S., Zhang, Z., Kim, M., Gunderson, C. W., Wang, Y.-P., Lenz, P., Yan, D., and Hwa, T. (2013).
417 Coordination of bacterial proteome with metabolism by cyclic AMP signalling. *Nature*, 500(7462):301–306.